Edinburgh Research Explorer

Experimental test on a fibre-reinforced scaled cross vault subjected to in-plane shear displacements at the springings

Experimental test on a fibre-reinforced scaled cross vault subjected to in-plane shear displacements at the springings

Simonetta Baraccani[1*], Lucia Zauli[1], DimitrisTheodossopoulos[2], Stefano Silvestri[1]

[1]*Department DICAM, University of Bologna, Italy*

[2]*ESALA, Edinburgh College of Art, University of Edinburgh, UK*

*corresponding author

Abstract

This work investigates the behaviour of unreinforced and reinforced cross vaults subjected to static shear deformation at the springings through an experimental campaign. An earlier companion paper discussed the results of a pseudo-static test performed on a 1:4 scaled model, built with timber blocks and lime mortar, applying shear displacements to two abutments until failure. This paper illustrates the effects of the same action applied to the same model after extrados reinforcement with Fibre Reinforced Polymer strips. Crack patterns and displacement evolution are presented and compared with those of the unreinforced model to evaluate the effectiveness of this seismic strengthening technique.

Keywords

Cross vault - Experimental test - Shear displacement - Springings - Fibre Reinforced Polymer

1. Introduction

Historical cultural heritage buildings are often characterized by different substructures that increase their structural complexity, including masonry arches, vaults (barrel vault, cross or groin vaults) and domes. Recent Italian seismic events have shown that masonry vaults, together with the facades of ancient churches, are among the most vulnerable elements [1],[2],[3],[4]. Analysis of the position and extent of damage in the vaults of churches revealed that, generally, the most critical vaults are those near the façade or perimeter walls [5],[6],[7]. In these cases, two of the vault's four springings are typically located on a stiff wall, whilst the other two on more flexible columns/walls. This leads to a strong difference in the lateral stiffness of the supporting structures (walls, piers, columns) that, during an earthquake, may cause significant global shear action on the whole vault. The pseudo-static

response of the vault induced by these imposed shear displacements at its springings often represents the predominant cause of damage/failure, overshadowing the dynamic response of the vault itself [8]. Moreover, a systematic collection of vault collapses after earthquakes [9] underlined that the vaults do not fail from their supports, but from their free height, as they are usually embedded into thick vertical elements and often filled with rubble material in the corner areas [10],[11],[12],[13].

To preserve significant elements like vaults and not compromise the architectural integrity of historical buildings, it is necessary to identify reliable yet unobtrusive and reversible reinforcement techniques, considering the additional demand of retaining the value of decorations that commonly cover the intrados. Traditional reinforcement techniques used in the past to strengthen the vaults are generally: metal ties or even arches across the supports, reinforced concrete screeds applied at the extrados, addition of material fill in the springing areas, placing steel cables alongside the extrados and construction of new ribs at the extrados [14],[15],[16]. These techniques may guarantee an adequate increment in strength, stiffness and ductility, but usually, especially the use of the concrete screeds, violate reversibility and conservation needs for historical monuments. Over the last 20 years, substantial research has taken place on the use of composite materials to strengthen historical masonry structures [17], in particular seminal work on portions of walls [18],[19], columns [20],[21], arches [22],[23], vaults and domes [24],[25],[26],[27],[28], [29],[30],[31],[32].

The benefits from the application of fibre reinforced polymers (FRP) for strengthening of masonry structures (easy installation, low self-weight and high strength, ability to preserve the initial geometrical configuration and reversibility) are fully appreciated. For vaults in particular, most of the experimental evidence has been produced for single-curvature arches or barrel vaults [22],[23],[24],[25],[26],[27],[28]. Among the parameters investigated (such as length and width of the strips, angle, type of loading, support conditions, type of fabric) one of the most important is the location of the FRP (intrados, extrados, or exactly at the expected failure points) as it affects the collapse mechanism and the ultimate failure load. Only few studies focus on the reinforcement with FRP of complex forms like cross-vaults or domes [29], [30]. In 2006 De Lorenzis et al. [29] presented an experimental demonstration on the reduction of the lateral thrust transmitted to the piers by a vault strengthened with FRP. Avorio, Borri et al. [32], [31], illustrated the application of FRP on the vaults of the town hall of Assisi and the San Barnaba church in Modena (at extrados). Foraboschi [22] developed collapse tests on masonry prototypes of brickwork arches, vaults and domes under a concentrated load, in both unreinforced and reinforced configurations, the latter with various types of FRP. To the best of the authors' knowledge, studies of the structural response of a FRP reinforced cross vault subjected to in plane shear displacements at the springings are not available in the scientific literature and this important action is investigated in this work.

The behaviour of a cross vault subjected to shear deformation at the springings has been investigated in a companion paper by the authors [8]. An experiment was developed on a 1:4 scaled model of a cross vault with in-plane shear displacement applied by laterally moving two abutments until failure, keeping fixed the other two. A pseudo-static displacement was imposed and, at each step, the cracks were recorded in terms of position, extension and opening width. Later, the model was rebuilt and reinforced through Kevlar aramid fibres and epoxy resin, and tested in the same way. This paper presents the results of the test on the reinforced model and their comparison with the behaviour of the previously tested unreinforced model, in terms of the detected crack pattern, the vertical and horizontal displacements of the transverse and longitudinal ridges, and the final collapse displacement. The objective is to estimate the effectiveness of this reinforcement technique and the structural behaviour of the strengthened vault. In addition, the detailed description of the experimental results may be useful to other researchers when calibrating their own numerical models. A short evaluation with a non-linear Finite Element Model (FEM) is made finally just to investigate the capabilities of commercial software accessible by practitioners in simulating the experimental results.

2. The earlier tests on the unreinforced scaled cross vault model

The physical model used throughout this series of tests was built using timber bricks and lime mortar mix [33]. The geometry of the cross vault is characterised by transverse arches span equal to 0.88 m, nave arch span equal to 1.10 m, and global rise around 0.76 m (Figure 1a). Subjecting this model earlier to in-plane shear displacement with no reinforcement highlighted that failure occurred essentially at 2.7% spread of the nave arch span (Figure 1b). This is in good agreement with results on similar cases available in the scientific literature [34], [35], [36]. More extensive insight to the experimental performance of the model can be found at the companion paper [8].
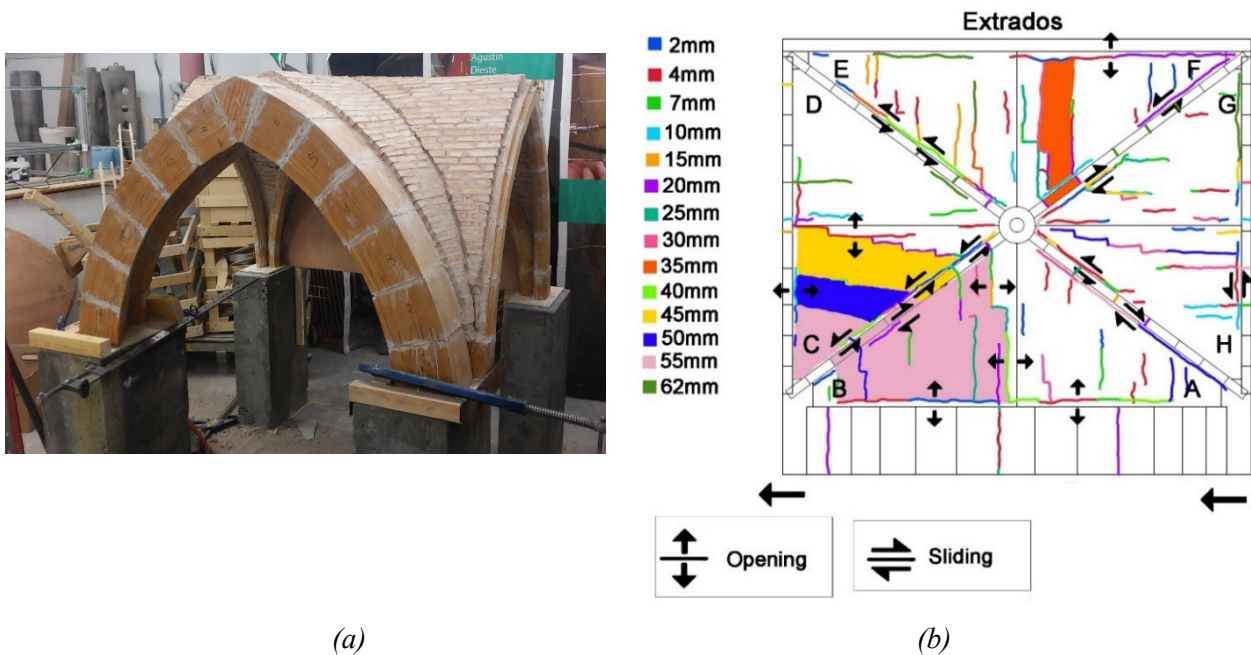
Fig. 1: *(a) The unreinforced scaled cross vault model, (b) extrados crack patterns at the main steps of lateral displacement of the two front supports [8].*
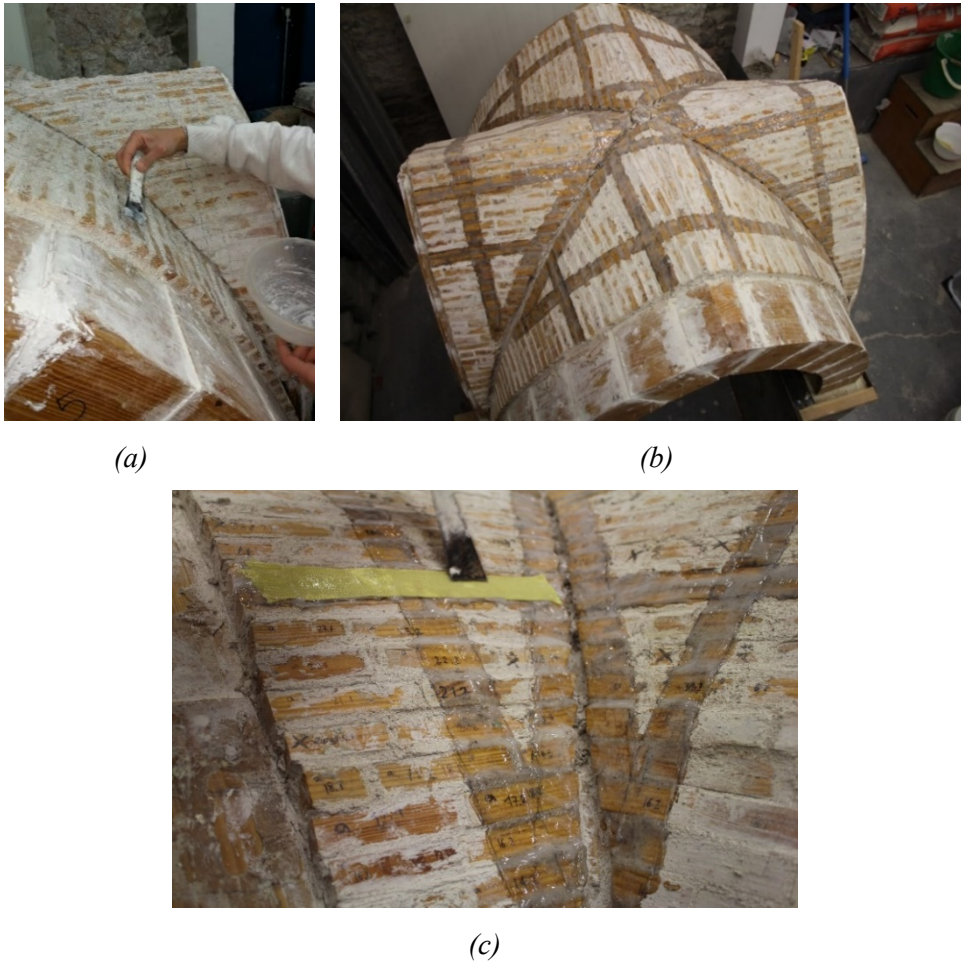
3. The reinforcement of the model

The physical model was rebuilt following the same steps described in the companion paper [8] and then reinforced with 40 mm-wide Kevlar aramid fibre bands applied on the extrados surface.

To fix the fibres to the timber bricks, a resin mix was prepared with (i) epoxy hardener, (ii) EL2 laminating epoxy, and (iii) fumed silica (introduced as extra material to increase stiffness). A typical proportion for the application was: three parts of Laminating epoxy, one part of epoxy hardener and a ratio of 2% - 3% (by weight) of fumed silica. First, two layers (Figure 2a) of a very viscous mixture were applied to homogenize (fill possible discontinuities) and prime the extrados of the bricks (provide a base level surface). Then, once dried, after 60-90 minutes, a third layer (Figure 2b) of epoxy was spread and the Kevlar aramid fibres were immediately positioned. Finally, a fourth layer of epoxy covered the fibres to obtain final saturation (Figure 2c). All these steps were carried out to guarantee adherence of the fibres to the structure.

The final result is shown in Figure 3: the fibres are located in the areas of the vault where the largest number of cracks was detected during the test on the unreinforced model [8]. The ends of the fibre bands did not reach the springings and the four perimeter arches, to assess the effectiveness of interventions in actual masonry vaults where the bands are not connected to the perimeter. This occurs in some vaults that have an incoherent solid fill in the corner areas and vertical masonry walls on the transverse arches, which prevent the application of reinforcement across them as their architectural integrity should be preserved by means of light, reversible and non-destructive interventions. Further

experimental tests are currently under consideration to assess the effectiveness of more invasive interventions like the removal of the solid fill in the corner areas and the anchorage of fibre bands all across the opposite perimeter walls.

(a)

(b)

(c)

Fig. 2: (a) First layer, (b) Third Layer, (c) Fourth layer.

(a)

(b)
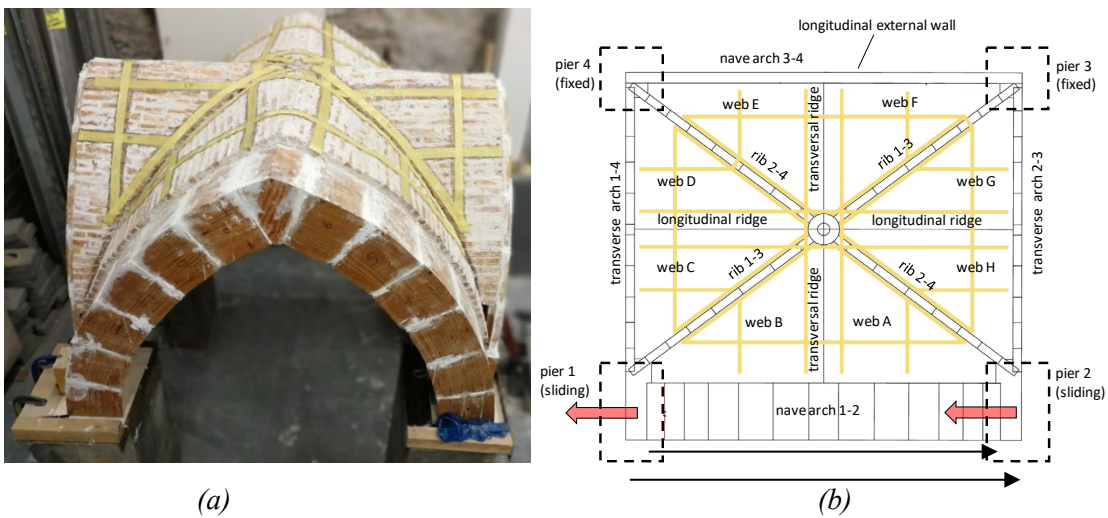
Fig. 3: (a) The reinforced model. (b) Plan view of the model with the fibre bands and the nomenclature of the structural elements.

4. The reinforcement material properties

Experimental tests were performed for the mechanical characterization of the materials used for strengthening the cross vault.

4.1. Tensile test on the fibre

To assess the tensile strength of the fibre as impregnated with resin, three bands of fibres rolled into epoxy were tested in direct tension. Each band was 140 mm-long and 40 mm-wide and its thickness was around 0.2 and 0.3 mm. Thus, the transverse section of each specimen was about 10 mm^2. Steel tabs were used to hold the fibres during the test. The displacement was recorded through a LVDT with a base length equal to 60 mm. Table 1 gives the main results of the three tensile tests. An average strength of about 1200 MPa, a Young modulus of about 38 GPa and a maximum displacement of about 2 mm were obtained.

Table 1: Maximum tension load, strength and Young modulus obtained in the three tension tests.

Test Number	Max load [kN]	Max displacement [mm] (base length = 60 mm)	Strength [MPa]	Young modulus [GPa]
Test 1	11.83	2.17	1183	32.7
Test 2	12.06	2.14	1206	33.8
Test 3	11.12	1.44	1112	46.3
Average	11.67	1.92	1167	37.6

4.2. Bonding test on the fibre-timber interface

To test the adherence strength of the fibre-timber interface, two specific specimens were prepared and tested. A fibre band was glued with epoxy to both sides of a 35 mm-wide timber brick and was put in tension until failure. The bonding area of each glued interface is equal to 2275 mm^2. Table 2 gives the main results of the two bonding tests. The failure mode of the shear test specimens was debonding of the fibre strip from the timber substrate with a thin epoxy-impregnated layer of timber included. An average adherence strength of about 1 MPa was obtained.

Table 2: Maximum bonding load and adherence strength obtained in the two bonding tests.

Test Number	Max load [kN]	Adherence strength [MPa]
Test 1	4273	0.94
Test 2	5112	1.12

5. The experimental test on the fibre-reinforced scaled cross-vault model

The setup and the procedure of the experimental test on the fibre-reinforced scaled cross-vault model are the same as the unreinforced one, see the companion paper [8]. Briefly, 5 mm steps of lateral displacements were applied on piers 1 and 2, by keeping fixed piers 3 and 4, thus introducing a shear deformation in the vault specimen (see Figure 3). A Total Station recorded the spatial displacements of selected extrados points (longitudinal and transverse ridges, transverse arches, nave arches, and webs A, B, C and H).

The crack pattern was observed on the extrados and the intrados after every spreading increment. In order to simplify the comprehension of the cracks' development, different colours are used for each step and thicker lines are adopted to represent the width of each crack (Figure 4). The detailed description of the cracking pattern is as follows:

- at the 5 mm stage of shear displacement, only cracks at the extrados were detected. The first, small, cracks initiated along the edge 3-4 and the transverse arches. A small fracture at the extrados appeared in the nave arch 1-2 near pier 1;

- the crack pattern at 10 mm showed the spreading of the perimeter cracks along the arches, while new cracks formed between the nave arch 1-2 and the two front webs A and B. Additional cracks appeared between voussoirs on the extrados of the nave arch 1-2. The diagonal rib 1-3 displayed the formation of two small hinges at the extrados with opening detectable at the intrados. From these first steps, it is clear that the cracks concentrated in the unreinforced portions of the model;

- at 20 mm, small cracks appeared at the extrados in both corner areas close to the sliding piers 1 and 2 (Figure 5a). The first cracks appeared at the intrados in web B and C close to the rib 1-3 where the fibre-bands ends. One of the existing extrados cracks in the left-hand side of the nave arch 1-2 increased until one voussoir started to slide downwards with respect to the adjacent one (Figure 5b);

- at 30 mm, the cracks along the wall edge 3-4 propagated and reached the two corner areas, involving also a small crack at the extrados of web D. The sliding voussoir of the nave arch 1-2 continued to move, followed by the whole left-hand side of the arch. At the intrados new cracks appeared between web A and the nave arch 1-2, and between web H and transverse arch 2-3;

- at 40mm, the detachment between the lower voussoir of the nave arch 1-2 and pier 1 increased. The cracks in the unreinforced corner areas increased both in their width and in their number. Although the central reinforced part of the vault was completely undamaged, the failure
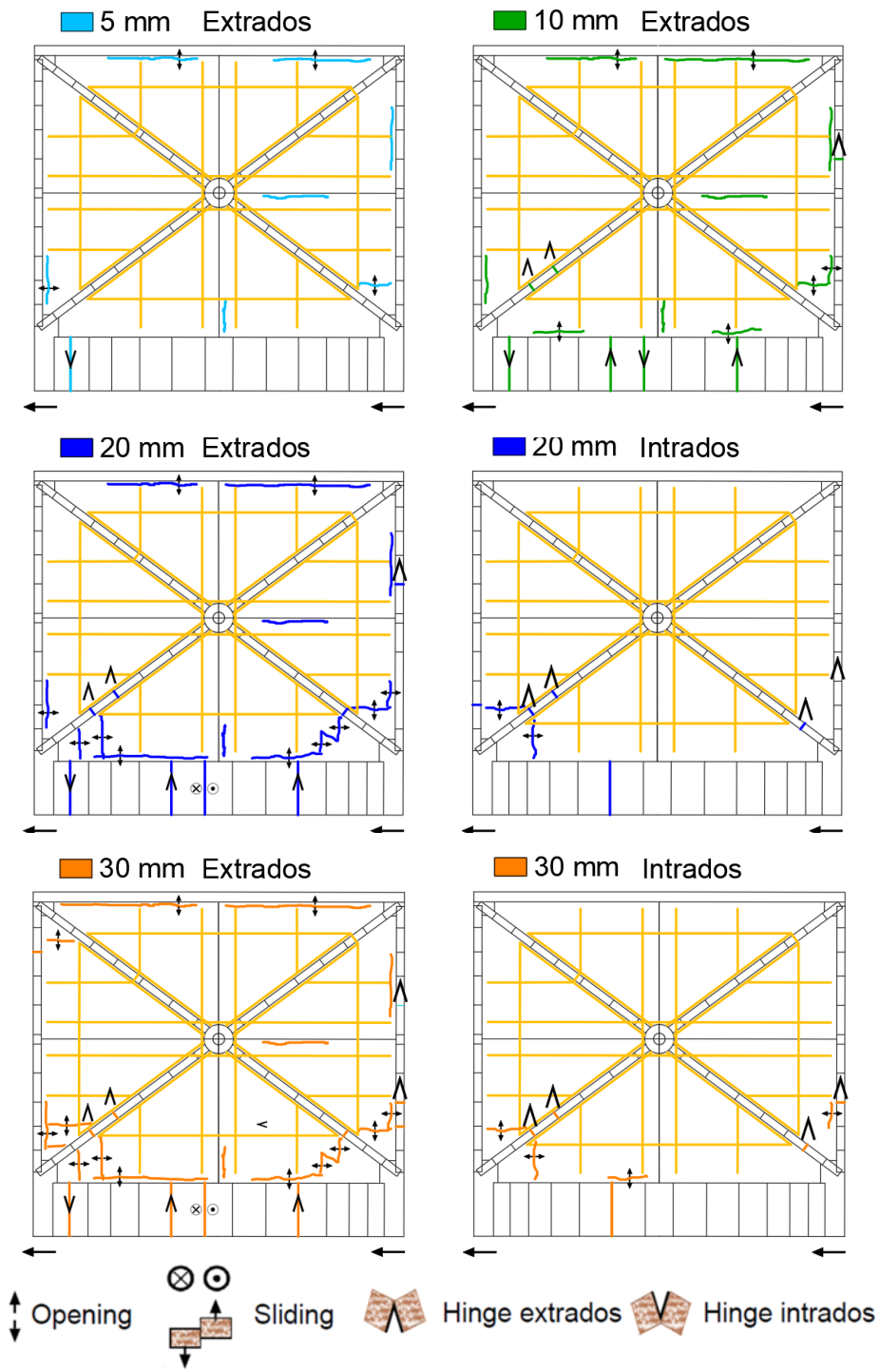
mechanism of the model started forming, defined by the dislocation of the voussoir of the nave arch 1-2 and the hinge on the intrados of the diagonal rib 1-3 (Figure 5c);
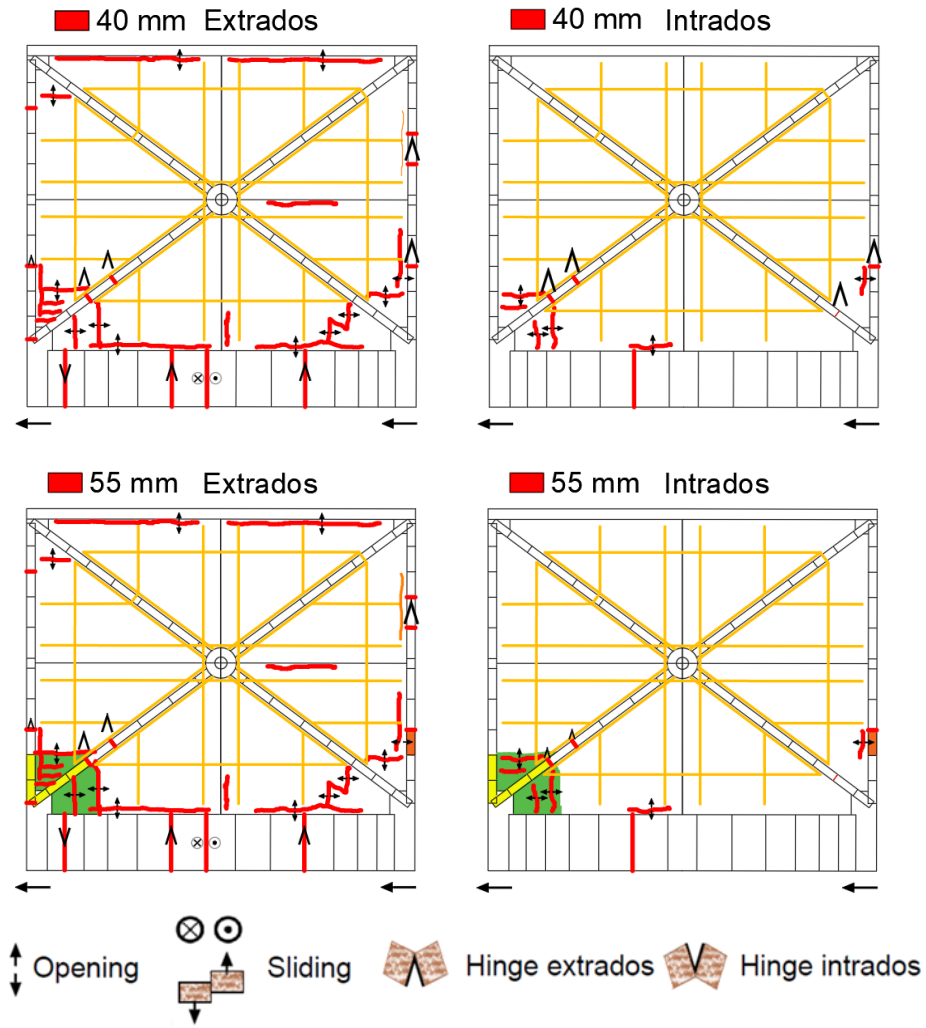
- for the successive displacement stages (45 and 50 mm) more damage occurred, especially in the unreinforced corner areas, but still the central strengthened portion of the vault remained undamaged (Figure 5d);

- at 55 mm, i.e. the last stage before collapse of the whole vault, the unreinforced corner area around pier 1 (webs B and C) started to collapse, involving voussoirs of the transverse arch 1-4 and the diagonal rib 1-3 (Figure 5e). In addition, one voussoir of the transverse arch 2-3 fell down (Figure 5f).

After this, the central strengthened portion of the vault was completely detached, found itself without supports and fell down. Table 3 summarises the main effects observed in the test.

Table 3: Summary of the main effects on the vault model.

Shear displacement of the abutments	Effects on the vault model
0 mm	-
5 mm	First crack formation along the perimeter
10 mm	Formation of small cracks in diagonal rib and nave arch
20 mm	Initiation of major cracks in the unreinforced corner area around piers 1 and 2
30 mm	Extension of the previous cracks
40 mm	Strong extension of all the existing cracks and development of new cracks in the unreinforced corner areas
55 mm	Partial collapse of the unreinforced corner area around pier 1
60 mm	Total collapse of the model

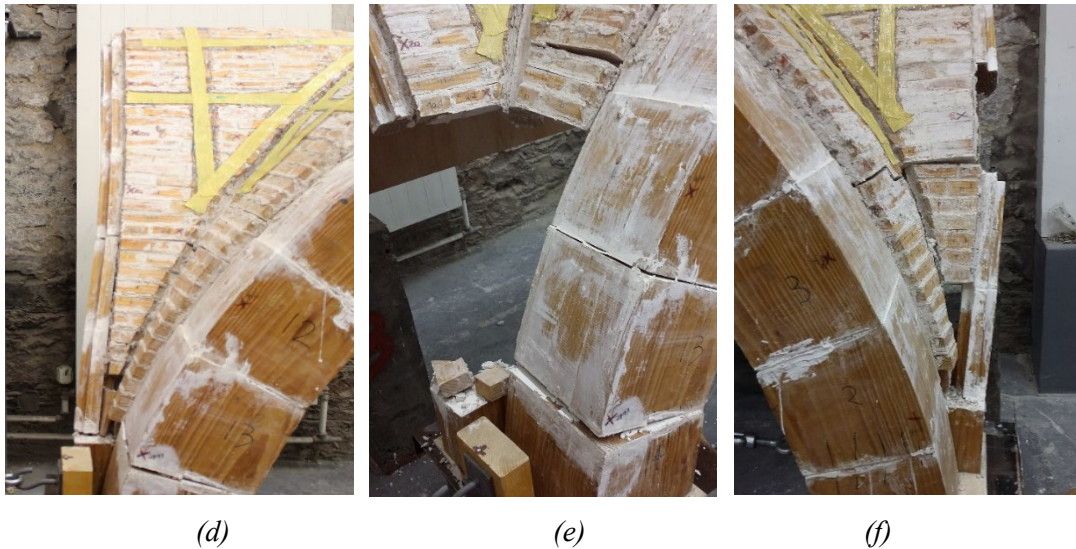5 mm   Extrados
10 mm   Extrados
20 mm   Extrados
20 mm   Intrados
30 mm   Extrados
30 mm   Intrados

Opening   ⊗ ⊙ Sliding   Hinge extrados   Hinge intrados

9

Fig. 4: *Crack pattern evolution and collapse condition.*

(a)   (b)   (c)

(d)	*(e)*	*(f)*

Fig. 5: *(a) Extrados cracks in the corner area close to pier 2. (b) Downwards sliding of the voussoir at the left of the keystone of nave arch 1-2. (c) Intrados cracks in the corner area close to pier 1. (d) Undamaged strengthened portion of the vault (webs B and C). (e) Collapse of the unreinforced corner area around pier 1. (f) Collapse of one voussoir of the transverse arch 2-3.*

## 6. Displacement results and their comparison between the unreinforced and reinforced models

In this section, the displacements of the reinforced (R) vault model are discussed and compared with those of the unreinforced (UNR) one. Only the most significant stages of the imposed shear displacement are discussed, namely 20, 30 and 40 mm, since 20 mm marks the initiation of major cracks and 40 mm is the last step before partial collapse, so no measurements were taken thereafter.

6.1. Vertical deflections of the transverse ridge

Figure 6 shows the vertical deflections of the transverse ridge with respect to the initial horizontal configuration (R - solid lines and UNR - dotted lines). In the reinforced case, after an initial general downward settlement of maximum 2 mm at the 5 mm, 10 mm and 20 mm stages of shear displacement, the global behaviour looks quite asymmetrical for the 30 mm and 40 mm stages. The points close to the back wall show small downward deflections, whilst the points close to the nave arch show large upward displacements up to 2 mm at the 30 mm stage and 5 mm at the 40 mm stage. The front portion, where the imposed shear-displacement is applied, lifts up.

The comparison of the two models, indicates that in the unreinforced case the behaviour is basically symmetrical across the ridge and the maximum deflection is reached at the keystone (around 12 mm). On the contrary, in the reinforced case the behaviour is almost asymmetrical and the most significant

deflection, although much less here (6 mm, i.e. half of the UNR maximum), is reached by the point on the nave arch.
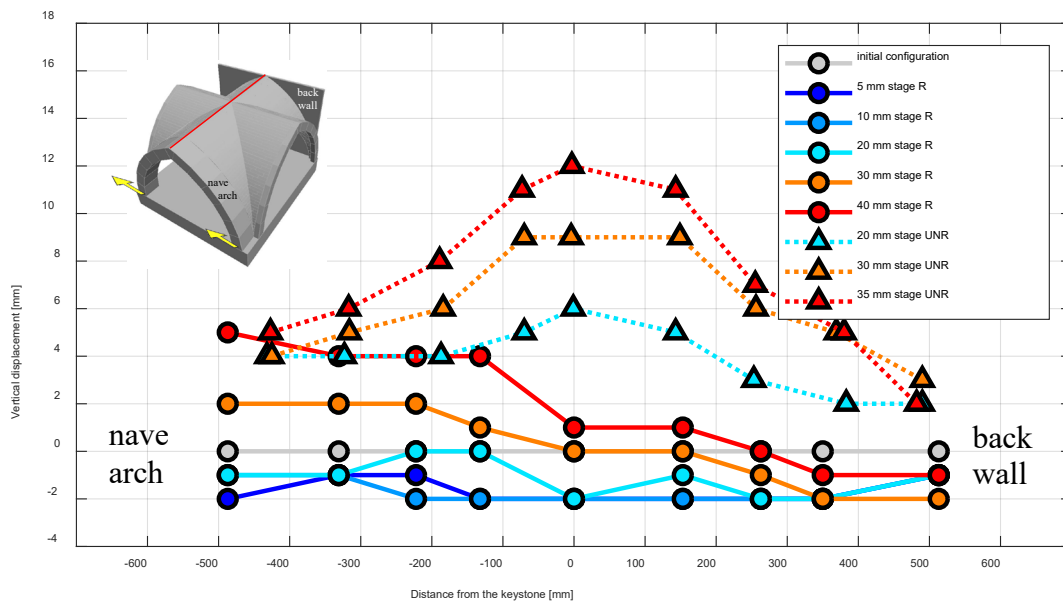
Fig.6: *Comparison of the vertical deflections of the transverse ridge for the unreinforced and reinforced models.*

6.2. Vertical deflections of the longitudinal ridge

Figure 7 shows the vertical deflections of the longitudinal ridge with respect to the initial horizontal configuration at selected displacement stages. In the reinforced case, as already observed for the transverse ridge, also the longitudinal ridge displays an initial downward displacement (again up to 2 mm) at the first stages (up to the 20 mm stage) and does not show a constant trend during all stages. At the 30 mm and 40 mm stages, the longitudinal ridge slightly rises; the maximum value is about 4 mm. It is evident that the displacements of the reinforced model are smaller than in the unreinforced model. The latter shows a clear symmetrical uplift of the central portion of the vault, up to 14 mm, whilst the former an upward movement of its portion closer to the transverse arch 2-3 around 2 – 4 mm.
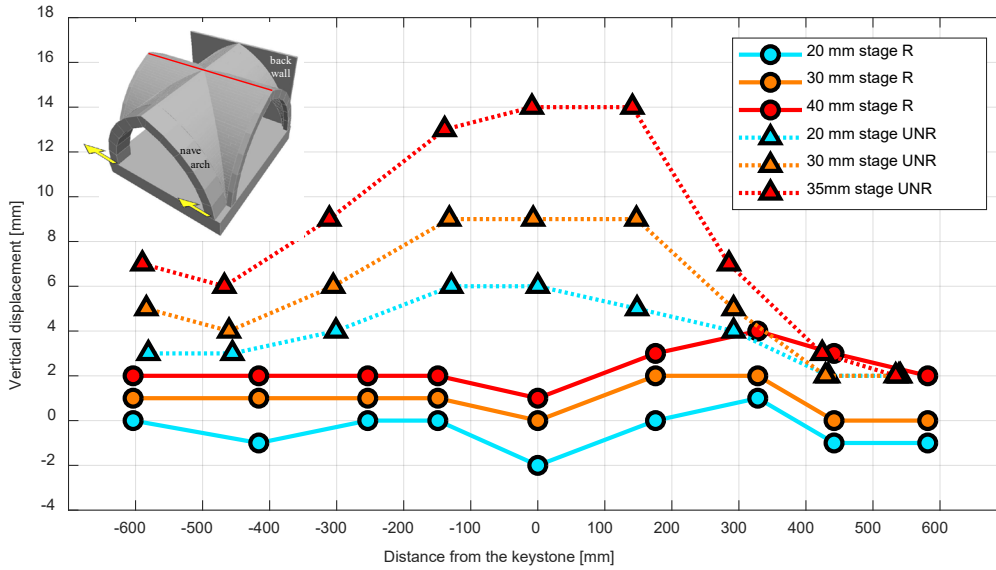
Fig. 7: Comparison of the vertical displacements of the longitudinal ridge for the unreinforced and reinforced models.
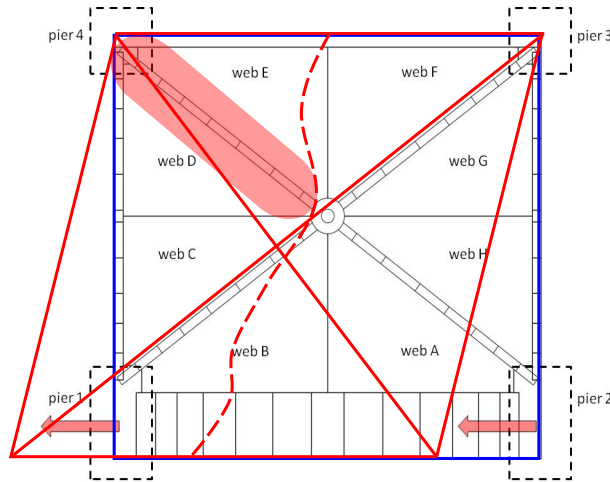
6.3. Horizontal displacements of the transverse ridge

It is important to study also the horizontal displacements of the transverse ridge with respect to the initial horizontal configuration, as a more direct effect of the in-plane shear displacement (Fig. 8). In general, the ridge seems to follow the imposed shear movement with larger displacement of the points close to the nave arch, up to 20-25 mm at the 30 mm and 40 mm stages, as expected due to the fact that this area is spreading. The recorded values of the displacements indicate that, at the first stages of shear movement (5 and 10 mm), the displacement of the transverse ridge is larger than the one imposed at the springings, whilst at the last stages (20, 30 and 40 mm) the displacement at the top is of the same order of magnitude as the imposed one at the bottom. The deformed shape clearly displays a hump, which is most probably due to the opposition provided by the compressed diagonal rib 2-4 and the surrounding webs D and E (Figure 9).

The difference (around 5 mm) between the lateral displacement of the last point of the transverse ridge at $y \cong$ -500 mm (as measured from the keystone) and the second last point at $y \cong$ -300 mm is consistent with the cracks that started developing at the 10 mm stage between the nave arch and the reinforced vault (Figure 4). All the more reason, the same consideration applies for the other side of the vault close to the back wall, which immediately detached from the reinforced vault even from the 5 mm stage (Figure 4): a final 10 mm difference can be observed between the points at $y \cong$ +500 mm and at $y \cong$ +350 mm from the keystone.
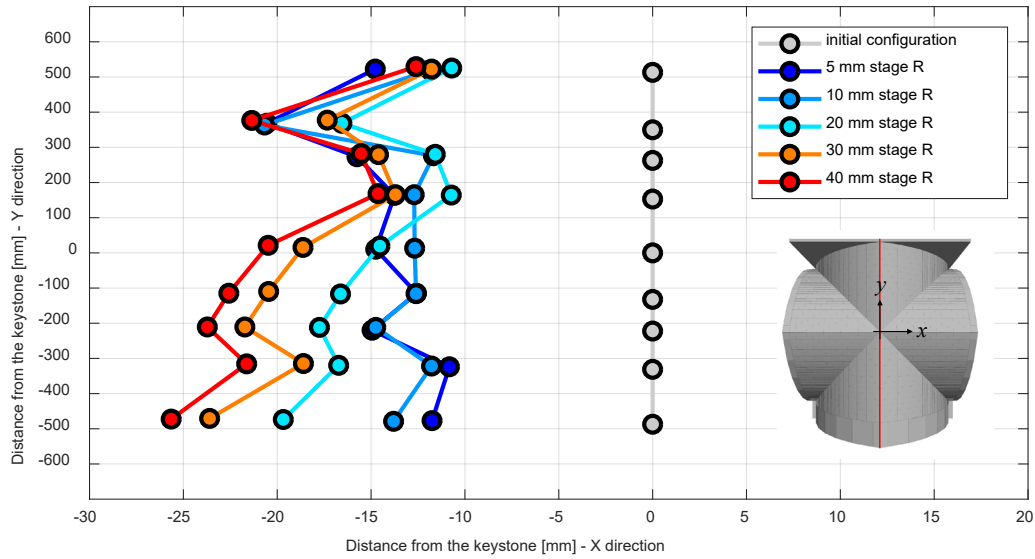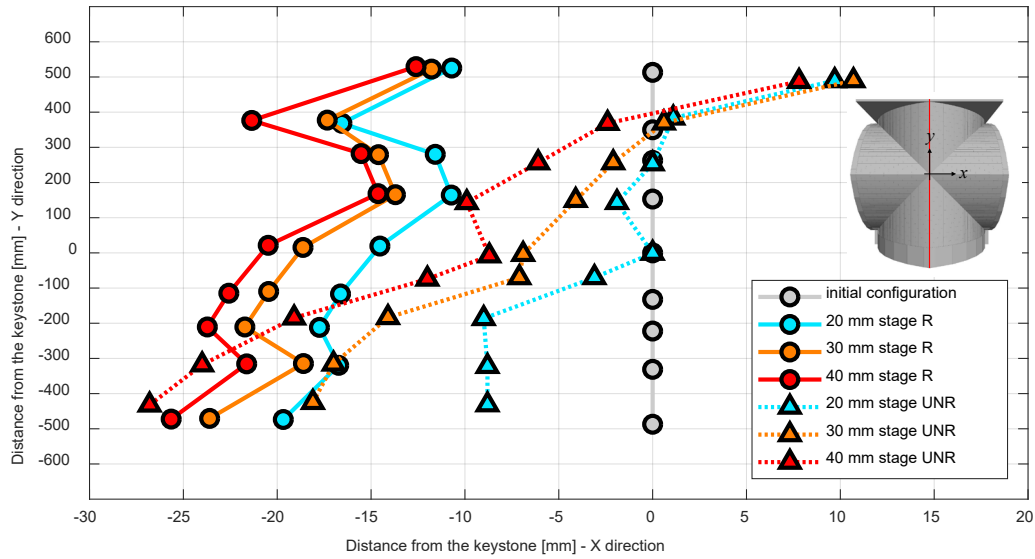
Fig. 8: *Horizontal displacements of the transverse ridge (plan view).*

Fig. 9: *Interpretation of the strut opposition provided by diagonal rib 2-4.*

Figure 10 compares the horizontal displacements of the transverse ridge for the two models. In both cases, the general lateral movement follows the imposed displacements at the springings with the largest displacements in the front side (nave arch), where a maximum value of around 25 mm was achieved. However, in the unreinforced case, the lateral movement is basically characterised by a global rotation of the transverse ridge towards a final diagonal configuration before the total collapse of the vault. On the contrary, in the reinforced case, the reinforcement makes the whole webs move as a block and the lateral movement is mainly described by a lateral (almost uniform, as compared with the unreinforced case) global translation that can occur due to the detachment of the bricks from the back wall and the frontal nave arch.
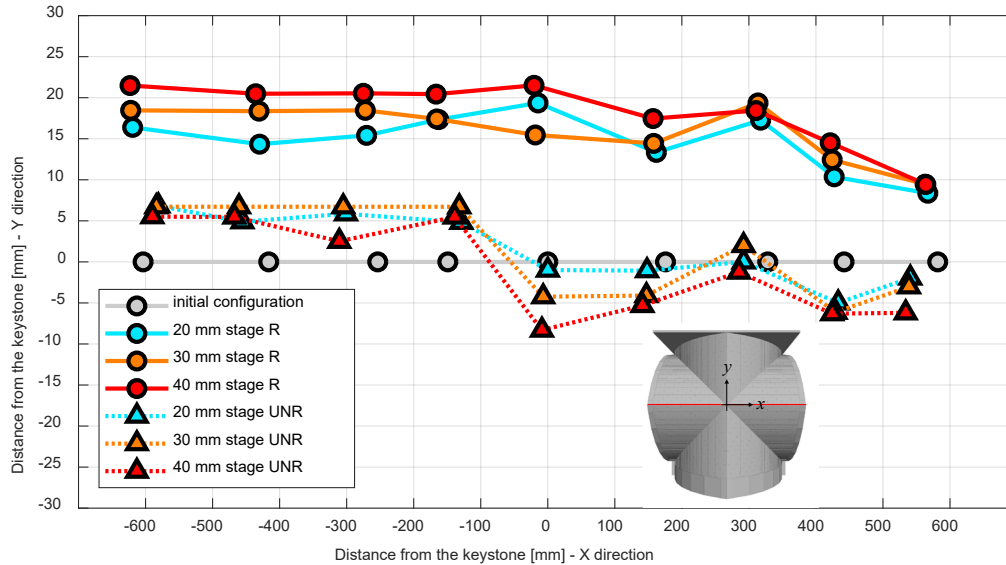
14

Fig. 10: *Comparison of the horizontal displacements of the transverse ridge for the unreinforced and reinforced models.*

6.4. Horizontal displacements of the longitudinal ridge

Figure 11 shows the horizontal displacements of the longitudinal ridge at selected shear displacement stages. In the reinforced case, the deformed shape consists of a roughly uniform translation towards the back wall. In more detail, the left portion of the longitudinal ridge moves slightly more than the right portion, maybe due to the fact that webs D and E are compressed and thus may shorten in plan. This last observation is also consistent with the hump characterising the deformed shape of the transverse ridge, detailed in Figure 9. The comparison of the two models indicate that in the unreinforced case the lower stiffness of the vault allows larger deformations to happen, so the left portion of the ridge moves towards the back wall and the right one opposite, with high concentration of strain and damage around the key-stone. On the contrary, in the reinforced case, the higher stiffness of the vault provided by the fibres make the ridge move together towards the back wall.

Fig. 11: *Comparison of the horizontal displacements of the longitudinal ridge for the unreinforced and reinforced models.*

6.5. Discussion

Figures 1b and 4 compare the crack patterns of the vaults in the unreinforced and reinforced configurations. It is clear that, in the unreinforced model, the cracks are almost uniformly distributed over the vault surface, whilst, in the reinforced one, the cracks developed only in the corner areas and no cracks occurred in the central portion of the vault where the fibres were placed.

Table 4 summarises the main effects observed on the two models and provides dimensionless shear displacement levels (with respect to the nave arch span 1.10 m) that can be useful as an indication of damage limits in real cross vaults. Both models reach the total collapse condition at about 5.5% of the longitudinal span (60 mm shear displacement). However, the way they reach the final collapse is completely different. On the one hand, the unreinforced model reaches partial collapses of the webs at about 3% of the longitudinal span (35 mm), thus indicating that (i) collapse is gradual (due to damage distribution all over the vault surface) and (ii) partial collapses associated with the falling of some blocks can occur thus compromising the safety conditions. On the other hand, the reinforced model maintains an undamaged central portion right until total failure, with the first partial damage (5%) of the corner unreinforced portions (close to the piers) appearing just before the total collapse (5.5%), thus indicating that (i) collapse is sudden (due to the final detachment of the central reinforced portion from the perimeter) and (ii) no blocks fall from the vault until shear displacement exceeds the 5% value of the longitudinal span.

This comparison clearly highlights the effectiveness of the fibre bands in the zones where they are placed and the criticalities in the unreinforced zones. This suggests that a more extensive intervention that would envisage fibre bands well anchored across all the perimetric edges may improve the

16

performance even more, by avoiding the development of mechanisms characterised by hinges in the springings [37].

Table 4: Comparison of the main effects on the unreinforced and reinforced vault models.

| Shear displacement stage	% Dimensionless shear displacement (with respect to the nave arch span)	Monitored effects on the unreinforced model	Monitored effects on the reinforced model
0 mm	0	-	-
4 - 5 mm	0.4%	Formation of small cracks	First crack formation along the perimeter
10 mm	0.9%	Initiation of small cracks in area	Formation of small cracks in diagonal rib and nave arch
20 mm	1.8%	Initiation of major cracks in webs B, C, F and G	Initiation of major cracks in the unreinforced corner area around piers 1 and 2
30 mm	2.7%	Extension of the major cracks	Extension of the major cracks in the unreinforced corner areas
35-40 mm	3.2% - 3.6%	Partial collapse of web F	Strong extension of the existing cracks and development of new cracks in the unreinforced corner areas
55 mm	5%	Partial collapse of the model: total collapse of webs B and C (around pier 1)	Partial collapse of the unreinforced corner area around pier 1
60 mm	5.5%	Total collapse of the model	Total collapse of the model

7. Finite Element modelling of the reinforced vault

Several advanced computational techniques have been developed to reproduce the response of arch and vault masonry structures, including Limit Analysis, Trust Network Method, Finite Element (FE) Method and Discrete Element Method approaches [38], [39], [40], [41], [42], [43], [44]. Since the purpose of this section is to explore the reliability of methods directly accessible by practitioners, embedded already in all-purpose commercial software, results obtained with a basic FE model are here presented.

The FE model used for the numerical non-linear analysis of the reinforced vault is the same as the one developed for the unreinforced vault (Figure 12a), described in the companion paper [8] and the Abaqus® [45] software was used. To represent the FRP reinforcement strips on the extrados surface, truss elements, characterised by the geometric and material properties described in sections 3 and 4, were added to the shell elements of the webs, by making reference to the nodes of the mesh and trying to match at best the exact location of the reinforcement strips (Figure 12b). The shearing deformation was applied with staged displacements imposed in piers 1 and 2 along the negative X direction until 40 mm.

Figure 13 shows the vertical displacements contour maps for the reinforced vault, whilst Figures 14a and b provide comparison between these data and the experimental ones. It can be noticed that:

- for large shear displacement stages (e.g. 30 and 40 mm), the qualitative response (upward movement of the points close to the nave arch) and the order of magnitude (around 5 mm) of the vertical displacements of the transverse ridge are well captured (Figure 14a). The vertical movements of the points close the back wall receive the effects of the boundary conditions (fixed restraints on the back perimeter arch, as per Figure 12), whilst the real vault experienced small downward movements;

- for large shear displacement stages (e.g. 30 and 40 mm), the qualitative response (upward movement) of the longitudinal ridge is captured (Figure 14b). From a quantitative point of view, due to the relatively small values of these displacements, this numerical model is not able to provide the order of magnitude;

- as it could be easily expected due to the unavoidable randomness of the real vault response to small displacement action, for the 20 mm stage, the numerical model cannot reproduce the experimental response at that stage but does simulate the qualitative response at larger displacements for both the transverse ridge and the longitudinal ridge.

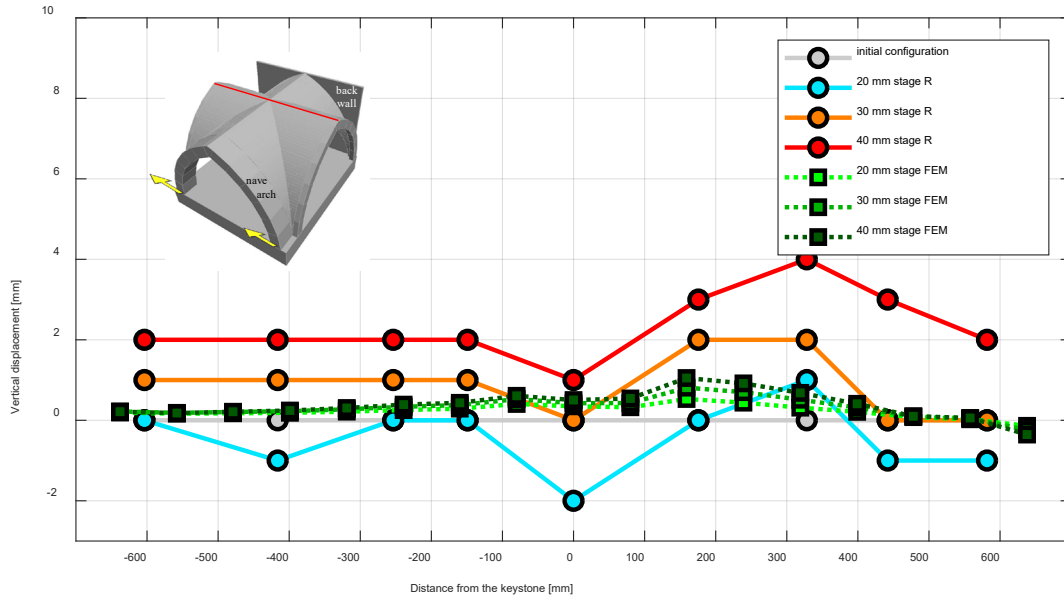*(a)*   *(b)*
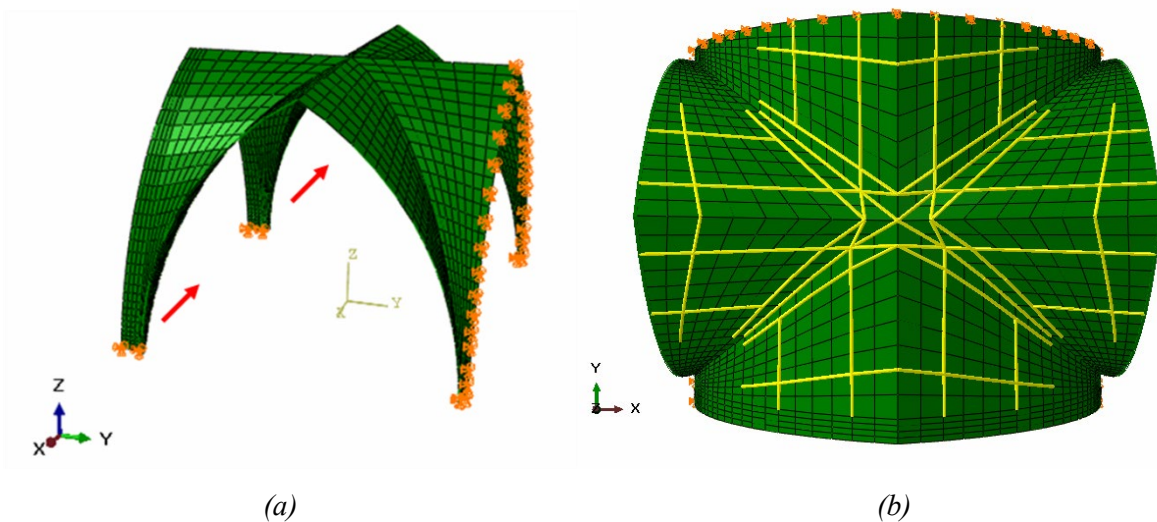
Fig. 12: *(a) 3D-view and (b) plan view of the numerical model of the vault without and with FRP reinforcement.*
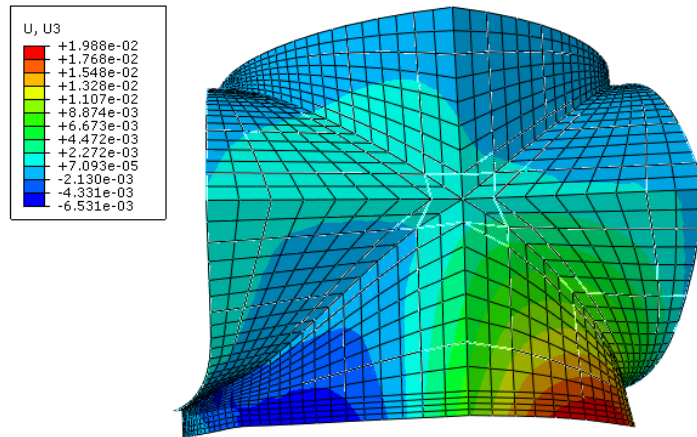
Fig. 13: *Contour map of the vertical displacements [m] in the FEM reinforced model (40 mm lateral displacement stage).*
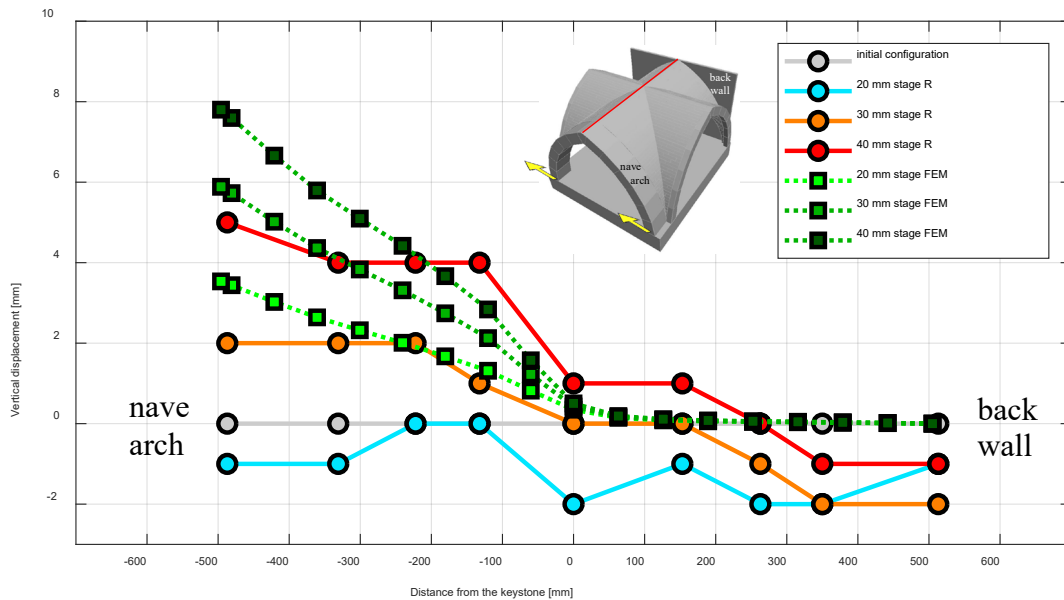

(a)

(b)

Fig. 14: Vertical displacements of (a) the transverse ridge and (b) the longitudinal ridge for the reinforced model: FEM numerical and experimental results.

The non-linear analysis using the Concrete Damage Plasticity model allows the tension damage variable (DAMAGET) contour plots to be obtained for the different shear displacement applied. Two illustrative plots are reported in Figure 15. The numerical results are in good agreement with the damage detected in the corner areas, capturing the damage occurred in the unreinforced lower part of the left front webs, as highlighted in Figure 5e. However, the numerical model indicates damages along the longitudinal ridge close to the key-stone that were not observed in the physical test. This may be due to the size and the shape of the shell elements near the keystone, that create a singular point characterised by sharp edges that may provoke stress concentrations in the numerical model. In the real vault model, the keystone is characterised by smooth curvatures (compare Fig. 2b with Fig. 12a).
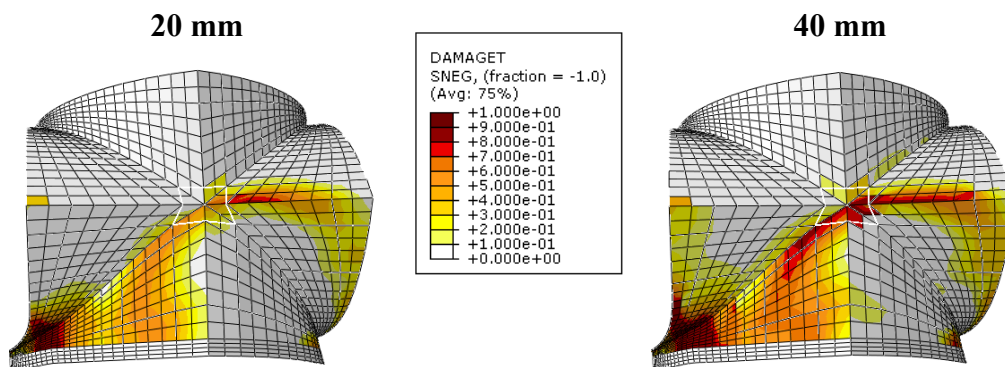
Fig. 15: Non-linear static damage contour plots in the FEM model.

8. Conclusions

This research work describes a pseudo-static test which constitutes the second step of an experimental campaign aimed at understanding the structural response of a cross-vault subjected to in-plane shear displacements at two springings, an action that represents the predominant earthquake effect on such structures, overshadowing the other effect represented by the dynamic response of the vault itself. The first step was concerned with a test developed on a bare 1:4 scaled cross-vault made up of timber blocks and lime mortar. This second step is focused on the same model reinforced through FRP strips on the extrados surface. The rationale behind the application of shear action lies in the higher vulnerability observed in the vaults near the façade or along the perimeter walls which are supported by structures characterised by different lateral stiffnesses.

Cracking patterns, vertical and horizontal displacements of the longitudinal and transverse ridges and collapse displacements have been recorded during the tests. A companion paper presented the results for the unreinforced model, whilst this paper presents the results for the reinforced one.

The two models show a similar collapse displacement, roughly around 5.5% of the nave arch span, but a completely different structural response. For the unreinforced model: collapse is gradual assisted by partial collapses (blocks falling from webs) observed starting from 3% spread of the longitudinal span. For the reinforced model: collapse is sudden and no damage is observed in the reinforced portion until total collapse.

Thus, from a seismic strengthening point of view, the application of the FRP reinforcement on the exposed surface of the vault extrados short off the springings (which would have included the removal of the rubble fill in real cases) allows the performance of the vault for low-moderate shear actions (i.e. frequent earthquakes) to improve, but does not affect the performance of these vaults under strong shear actions (i.e. rare earthquakes). In order to increase the effectiveness of this strengthening technique under stronger motions, an intervention that sees fibre bands well anchored to all the perimetric edges may be considered. A third test with this solution is currently under consideration.

9. References

[1] S. Lagomarsino, "Damage assessment of churches after L'Aquila earthquake (2009)," *Bull. Earthq. Eng.*, vol. 10, no. 1, pp. 73–92, 2012.

[2] S. Lagomarsino and S. Podestà, "Seismic vulnerability of ancient churches: I. Damage assessment and emergency planning," *Earthq. Spectra*, vol. 20, no. 2, pp. 377–394, 2004.

[3] F. Parisi, F. De Luca, F. Petruzzelli, R. De Risi, and E. Chioccarelli, "Field inspection after the May 20th and 29th 2012 Emilia-Romagna earthquakes," 2012.

[4] M. Dolce *et al.*, "The Emilia Thrust Earthquake of 20 May 2012 (Northern Italy): Strong Motion and Geological Observations - Report 1 -," vol. 2012, pp. 1–12, 2012.

[5] G. Basile, *Restauri in San Francesco ad Assisi: Il cantiere dell'utopia : studi, ricerche e*

interventi sui dipinti murali e sulle vetrate dopo il sisma del 26 settembre 1997. Perugia, Italy: Quattroemme, 2007.

[6] S. Baraccani *et al.*, "A Structural Analysis of the Modena Cathedral," *Int. J. Archit. Herit.*, vol. 10, no. 2–3, 2016.

[7] G. Croci, "General methodology for the structural restoration of historic buildings: The cases of the Tower of Pisa and the Basilica of Assisi," *J. Cult. Herit.*, vol. 1, no. 1, pp. 7–18, 2000.

[8] C. Carfagnini, S. Baraccani, S. Silvestri, and D. Theodossopoulos, "The effects of in-plane shear displacements at the springings of Gothic cross vaults," *Constr. Build. Mater.*, vol. 186, pp. 219–232, 2018.

[9] J. V. Ochoa Romá, S. Supervisor: Silvestri, and S. Co-supervisor: Baraccani, "Shaking Table Tests and DEM Numerical Modeling of a 3D-Printed Groin Vault," 2019.

[10] G. Croci, "The collapses occured in the basilica of St. Francis of Assisi and in the cathedral of Noto," *Struct. Anal. Hist. Constr. II*, 1998.

[11] E. Piermarini, "The Dynamic Behavior of the Basilica of San Francesco of Assisi," 2013.

[12] C. Cancino, S. Farneth, P. Garnier, J. Vargas, and F. Webster, *Estudio de daños a edificaciones históricas de tierra después del terremoto del 15 de agosto del 2007 en Pisco, Perú*. 2009.

[13] T. Basiricò, S. Campione, and A. Cottone, "Partial collapse and reconstruction of the vault of the Cathedral in Piazza Armerina (Sicily, Italy)," 2016, no. January.

[14] P. Napoli, "Rinforzo Di Archi E Volte." pp. 1–17.

[15] L. Jurina, "The 'reinforced arch method': a new technique in static consolidation of arches and vaults.," in *Proc. of the European Conference "Innovative Technologies and Materials for the Protection of Cultural Heritage.,"* 2003.

[16] L. Ferrario, M. Alessandra, V. Andreis, S. Zanotti, P. Riva, and E. Giuriani, "Behavior and retrofitting of single-leaf vaults under distributed horizontal forces," in *Structural Analysis of Historical Constructions –Jerzy Jasieńko (ed)*, 2012.

[17] A. Grazzini and S. Agnetti, "Post-seismic effectiveness of the strengthening work carried out with FRP applied to historical masonry buildings: the case study of the Spoleto Cathedral," *Compos. Mater. Res.*, vol. 7, no. 1, pp. 1–11, 2019.

[18] M. Corradi, A. Borri, and A. Vignoli, "Strengthening techniques tested on masonry structures struck by the Umbria-Marche earthquake of 1997-1998," *Constr. Build. Mater.*, vol. 16, no. 4, pp. 229–239, 2002.

[19] M. R. Valluzzi, D. Tinazzi, and C. Modena, "Shear behavior of masonry panels strengthened by FRP laminates," *Constr. Build. Mater.*, vol. 16, no. 7, pp. 409–416, 2002.

[20] M. A. Aiello, F. Micelli, and L. Valente, "Frp confinement of square masonry columns," *J. Compos. Constr.*, vol. 13, no. 2, pp. 148–158, 2009.

[21] A. Parvin and D. Brighton, "FRP composites strengthening of concrete columns under various loading conditions," *Polymers (Basel).*, vol. 6, no. 4, pp. 1040–1056, 2014.

[22] P. Foraboschi, "Strengthening of Masonry Arches with Fiber-Reinforced Polymer Strips," no. June, pp. 191–202, 2004.

[23] D. V. Oliveira, I. Basilio, and P. B. Loureņo, "Experimental behavior of FRP strengthened masonry arches," *J. Compos. Constr.*, vol. 14, no. 3, pp. 312–322, 2010.

[24] M. R. Valluzzi, M. Valdemarca, and C. Modena, "Behavior of Brick Masonry Vaults Strengthened by FRP Laminates," *J. Compos. Constr.*, vol. 5, no. 3, pp. 163–169, 2002.

[25] M. Corradi, A. Borri, G. Castori, and K. Coventry, "Experimental analysis of dynamic effects of FRP reinforced masonry vaults," *Materials (Basel).*, vol. 8, no. 12, pp. 8059–8071, 2015.

[26] G. Ramaglia, G. P. Lignola, A. Balsamo, A. Prota, and G. Manfredi, "Seismic Strengthening of Masonry Vaults with Abutments Using Textile-Reinforced Mortar," *J. Compos. Constr.*, vol. 21, no. 2, pp. 1–16, 2017.

[27] F. G. Carozzi, C. Poggi, E. Bertolesi, and G. Milani, "Ancient masonry arches and vaults strengthened with TRM, SRG and FRP composites: Experimental evaluation," *Compos. Struct.*, vol. 187, no. October 2017, pp. 466–480, 2018.

[28] L. Garmendia, P. Larrinaga, R. San-Mateos, and J. T. San-José, "Strengthening masonry vaults with organic and inorganic composites: An experimental approach," *Mater. Des.*, vol. 85, pp. 102–114, 2015.

[29] L. De Lorenzis, R. Dimitri, and A. La Tegola, "Reduction of the lateral thrust of masonry arches and vaults with FRP composites," *Constr. Build. Mater.*, vol. 21, no. 7, pp. 1415–1430, 2007.

[30] A. Avorio, A. Borri, and M. Bottardi, "Theoretical Analysis and a case study of historical masonry vault strengthened by using advanced FRP," in *3rd International Conference Advanced Composite Materials in Bridge and Structures*, 2000.

[31] A. Borri, M. Corradi, and A. Vignoli, "Seismic upgrading of masonry structures with FRP," *… 'Degli Stud. di Perugia, Fac. di …*, 2002.

[32] A. Avorio, A. Borri, M. Corradi, A. Barbieri, and A. Di Tommaso, "Comportamento dinamico di volte in muratura rinforzate con FRP-materials: primi risultati," in *X Congresso Nazionale "L'ingegneria Sismica in Italia" ANIDIS*, 2001, no. January 2016.

[33] D. Theodossopoulos, "Structural behaviour of historic masonry cross vaults," 2002.

[34] M. Rossi, C. Calderini, and S. Lagomarsino, "Experimental testing of the seismic in-plane displacement capacity of masonry cross vaults through a scale model," *Bull. Earthq. Eng.*, vol. 14, no. 1, pp. 261–281, 2016.

[35] G. Milani, M. Rossi, C. Calderini, and S. Lagomarsino, "Tilting plane tests on a small-scale masonry cross vault: Experimental results and numerical simulations through a heterogeneous approach," *Eng. Struct.*, vol. 123, pp. 300–312, 2016.

[36] A. Gaetani, "Seismic performance of masonry cross vaults: learning from historical developments and experimental testing," *PhD Thesis,University Minho*, 2016.

[37] A. Borri and G. Castori, "Interventi con AFG sulle volte di Palazzo Jacobili in Foligno," 2002.

[38] J. Heyman, *The stone skeleton:structural engineering of masonry architecture*. Cambridge University Press, 1995.

[39] A. Tralli, C. Alessandri, and G. Milani, "Computational Methods for Masonry Vaults: A Review of Recent Results," *Open Civ. Eng. J.*, vol. 8, no. 1, pp. 272–287, 2014.

[40] P. Roca, M. Cervera, G. Gariup, and L. Pela', "Structural analysis of masonry historical constructions. Classical and advanced approaches," *Arch. Comput. Methods Eng.*, vol. 17, no. 3, pp. 299–325, 2010.

[41] E. Milani, G. Milani, and A. Tralli, "Limit analysis of masonry vaults by means of curved shell finite elements and homogenization," *Int. J. Solids Struct.*, vol. 45, pp. 5258–5288, 2008.

[42] B. Pulatsu, E. Erdogmus, E. M. Bretas, and P. B. Lourenco, "In-plane static response of dry-joint masonry arch-pier in-plane static response of dry-joint masonry arch-pier," in *AEI 2019 : Integrated Building Solutions—The National Agenda*, 2019, no. April.

[43] H. Alexakis, N. Makris, and M. Asce, "Hinging Mechanisms of Masonry Single-Nave Barrel Vaults Subjected to Lateral and Gravity Loads," *J. Struct. Eng.*, 2017.

[44] D. Foti, V. Vacca, and I. Facchini, "DEM modelling and experimental analysis of the static behavior of a dry-joints masonry cross vaults," *Constr. Build. Mater.*, 2018.

[45] "Abaqus®. Theory manual, version 6.14." 2014.